ELSEVIER

Contents lists available at ScienceDirect

Electrochimica Acta

journal homepage: www.journals.elsevier.com/electrochimica-acta



Electrodeposition of ReMo alloys

Quanhong Liu, Qiang Huang

Department of Chemical and Biological Engineering, The University of Alabama, Tuscaloosa, AL 35487, USA

ARTICLE INFO

Keywords: Electrodeposition Rhenium molybdenum alloys Superconducting Amorphous superconductor Oxometallate citrate

ABSTRACT

The electrodeposition of superconducting ReMo alloys is investigated using highly concentrated electrolytes with acetate, citrate, and the two oxometallate anions, MOO_4^{2-} and ReO_4^{-} . The effects of applied deposition current, the concentrations of acetate, citrate, and metal source in the electrolyte on the film composition, faraday efficiency as well as the partial current densities of Re and Mo are systematically studied. A hybrid complex species, such as $(MOO_4^{2-})(ReO_4^{-})(HCit^{3-})_2$ and its partially reduced form, is proposed to form and mediate the co-deposition reaction. The morphology and superconductivity of alloy films are characterized using microscopy and cryogenic four-probe measurements. The electrodeposited ReMo alloy films maintain the same amorphous grain structure and the same enhanced superconducting transition temperature as pure Re films.

1. Introduction

Rhenium, a 5d transition metal in the VIIB group, is distinguished by its exceptional properties, including a high density, a high melting temperature, and a very rich variety of oxidation states [1]. These characteristics render it an invaluable material in high-temperature machinery and aeronautic constructions [2]. In its alloy forms with other metals, Re is also used in catalysts to enhance the efficiency and selectivity in various chemical synthesis and conversion reactions [3,4]. On the other hand, molybdenum is a 4d VIB transition metal also known for its exceptional mechanical properties appealing to the manufacturing industry, such as automobiles and aerospace. The rich chemistry and unique physical properties of Mo metal and its compounds also bring interest from chemical or electrochemical catalysis, microelectronics, and semiconductors [5-10].

The interest of Re further extends into the realm of superconductivity for potential applications in cryogenic electronics [11-13]. As type I superconductors, Re and Mo in their bulk crystalline form have a critical temperature (T_c), or a superconducting transition temperature, of 1.7 and 0.9 K, respectively [14]. However, the same metals in their amorphous forms, i.e., with extremely refined grains, present different critical temperatures due to a change in the density of state at the grain surfaces [15]. Such a deviation from the bulk behavior was found to strongly depend on the number of valence electrons, with the maximum improvement in critical temperature observed between 6 and 7 electrons per atom [16]. Mo and Re have 6 and 7 valence electrons, respectively, and the alloying between the two provides a unique

opportunity to tune this number and achieve the maximum. On the other hand, the thermodynamically stable crystalline ReMo alloy system has a rich phase diagram [17] and enhanced critical temperatures up to 14 K have been reported for certain compositions and crystalline phases [18-20]. Therefore, ReMo alloy would be of great interest as a better alternative to Re with enhanced superconductivity. However, the superconducting metals and alloys, including the ReMo, are typically prepared with vacuum deposition methods or high temperature metallurgical processes such as melting, casting, and sintering [21,22].

Electrodeposition is a cost-effective method for thin film fabrication, which can be easily scaled up and adapted to substrates with arbitrary geometries. Electrodeposition of superconducting elemental Re has been recently reported, where amorphous Re is obtained with an enhanced T_c of 6 K [23]. However, this enhancement is deminished upon recrystallization during thermal treatment [24]. Electrodeposition of superconducting Re alloys with iron-group metals have also been reported in attempt to tune the thermal stability of T_c. However, the superconductivity of these alloy films is compromised, where the Tc significantly decreases upon the inclusion of merely a few percent of the magnetic iron-group metals [25,26]. On the other hand, an enhanced deposition rate of Re is also observed [27,28]. Such a facilitated deposition, which sometimes is called induced deposition behavior, has also been observed when group VIB/VIIB metals such as Mo, W, Re, or Mn are co-deposited with iron-group metals [29-32]. However, to the best of our knowledge, alloys of VIB/VIIB metals alone, such as the binary alloys of Re and Mo, have never been electrodeposited. In fact, studies on electrochemical co-deposition of alloys often involve at least one simple metal cation and

E-mail address: qhuang@eng.ua.edu (Q. Huang).

^{*} Corresponding author.

the co-deposition using only oxometallate anions has never been reported.

In our previous studies [33], the electrodeposition of metallic Mo using highly concentrated acetate solutions, so called water-in-salt electrolytes, has been systematically investigated. On the other hand, Re metal and Re alloys with Fe and Co have also been electrodeposited using water-in-salt electrolytes [25]. While the incorporation of Fe inhibits the Re recrystallization at high temperature, it also significantly compromises the $T_{\rm c}$ [26]. This work further extends the learning to Re-Mo alloy system. Efforts in this study are focused on the development of electrolytes and the understanding of the alloy co-deposition behavior. The underlying mechanism for the observation will also be attempted.

2. Experimental

2.1. Electrolytes

Ammonium perrhenate (NH₄ReO₄, 99.9 %), sodium molybdate dihydrate (Na₂MoO₄, 99.5 %), lithium acetate (LiAc, CH₃COOLi, 98 %), potassium acetate (KAc, CH₃COOK, 99 %), ammonium acetate (NH₄Ac, CH₃COONH₄, 97 %), potassium chloride (KCl, 99 %), and citric acid (C₆H₈O₇, 99.5 %) are used to prepare all the electrolytes used in this study. All solutions are prepared at an elevated temperature of 35 °C with vigorous stirring and cooled down to a room temperature of 20 °C before any measurements or studies. Deionized (DI) water with a resistivity of 18.2 Mohm-cm is used. The pH of electrolytes is measured using Thermo Fisher Orion Star A211 pH meter. The natural pH's of electrolyte are listed in Table 1 and are used without further adjustment. Almost all solutions have a pH between 6 and 7, except for one solution without acetate, which will be discussed in the results. The viscosity of electrolytes are measured using Viscolite-700HP Laboratory Viscometer System, and the kinematic viscosity is between 10 and 14 cP for all the solutions except for the one without acetate. All deposition studies are carried out using a solution volume of 100 mL and at a room temperature of 20 $^{\circ}$ C.

2.2. Electrochemical cell

A traditional home-made cell with three compartments is used to conduct all electrochemical studies. The reference electrode is a silver chloride (Ag/AgCl) electrode saturated with KCl (0.197 V vs. NHE) placed in the reference compartment connected to the catholyte through

a capillary. All potentials are referred to with respect to this Ag/AgCl in this work. A 99.99 % platinum foil is used as the counter electrode in the anolyte compartment separated from the catholyte with a glass frit to prevent intermixing between anolyte and catholyte. Rotating copper discs with a diameter of 5 mm or a surface area of 0.196 cm² are used as working electrodes to prepare films for microscopic and spectroscopic characterizations. A fixed rotation speed of 1000 rpm is used in this work to provide agitation, to maintain the homogeneity of the solution, and to dislodge hydrogen bubbles from the electrode surface. Silicon coupons with gold strip patterns are used to deposit film for superconductivity measurements. The details of the pattern and the fabrication have been reported previously [24]. The coupon is mounted on a rotating electrode holder with front electrical contact and is electrodeposited in a same fashion as a rotating disc electrode. Cu and Au substrates are used as they don't form intermetallic compounds with Re or Mo and they are easily available. They are also commonly used for electrodeposition for metal and alloy thin films as the nucleation overpotential on them is relatively low, facilitating the nucleation and coalescence of thin film.

The conductivity of electrolytes is measured using a cylindrical tubular glass cell with two parallel Ti plates at both ends. The diameter of the cell is about 5 mm and the total volume is about 2 mL. A standard 0.1 M KCl solution with a known conductivity of 11.616 mS/cm [14] is used to calibrate the cell. Electrochemical impedance spectra are acquired for the electrolytes. The solution resistances are determined on Nyquist diagram, where the imaginary impedance is 0, and are used to calculate the conductivity by scaling with the standard KCl solution.

2.3. Instrumentation

A PINE research MSR electrode rotator is used to control the agitation in this work. An Autolab 302 N potentiostat with a frequency analyzer is used for all electrochemical studies. Electrochemical impedance spectra of solutions are acquired using a sinusoidal potential wave with an amplitude of 10 mV and a frequency sweep from 100 kHz to 0.1 Hz, superimposed on a DC bias slightly cathodic to the open circuit potential. The partial current density and faradaic efficiency of deposition are calculated from the deposit thickness and the chemical composition of the deposit, which are determined with a Bruker Mistral X-ray fluorescence spectroscope (XRF) operated with a 0.7 mm collimator and at 50 kV. Five points are evenly spaced across the diameter of the Cu disc electrode. The average thickness across these five locations is used. The average film composition is reported as atomic percent, which

Table 1
Summary of electrolytes used in this study.

	$\mathrm{NH_{4}ReO_{4}}$	$NaMoO_4$	$\mathrm{CH_{3}COOLi}$	CH ₃ COONH ₄	$C_6H_8O_7$	pН	conductivity
Effects of acetates	20 mM	50 mM	0	0	0.4 M	2.12	10.8
			0.5 M	8.5 M		6.46	33.3
Effects of citric acid	20 mM	50 mM	0.5 M	8.5 M	0	NA	NA
					0.1 M	7.12	44.5
					0.2 M	6.71	39.9
					0.4 M	6.46	34.5
					0.7 M	6.28	25.4
					0.9 M	6.16	19.8
Effects of ReO ₄	0	50 mM	0.5 M	8.5 M	0.4 M	6.47	34.5
	5 mM					6.45	34.3
	10 mM					6.43	34.1
	20 mM					6.46	33.3
	30 mM					6.50	31.9
	50 mM					6.41	30.5
Effects of MoO ₄ ²	20 mM	0	0.5 M	8.5 M	0.4 M	6.37	34.7
		10 mM				6.52	34.6
		20 mM				6.40	33.9
		30 mM				6.41	33.0
		50 mM				6.46	31.5
		70 mM				6.48	30.8

Q. Liu and Q. Huang Electrochimica Acta 500 (2024) 144761

is converted from the weight percent by XRF. The film surface morphology is characterized using a Thermo Fisher Apero Field Emission Scanning Electron Microscope (FE-SEM) operated at 20 kV. The superconductivity of electrodeposited films is characterized using a Quantum Design Dynacool Physical Property Measurement System (PPMS). The superconducting critical temperature or transition temperature is determined by recording the film resistance along with temperature sweep from 30 K to 1.8 K. A four-probe configuration is used for the resistance measurement. Dupont 4929NTM silver paint and aluminum wires are used to form four connections between the film and the resistivity puck.

3. Results and discussion

3.1. Electrolyte development

While the electrolyte chemistry has been listed in the experimental section, it is worth reporting the learning during the electrolyte development for alloy deposition. Our previous studies show that Re deposition from water-in-salt electrolytes with superhigh concentration of LiCl results in films with improved morphology and enhanced superconductivity [23,34]. On the other hand, the electrodeposition of metallic Mo can be achieved when a superhigh concentration of acetates are present in electrolytes [35-38]. A combination of both potassium acetate (CH3COOK) and ammonium acetate (CH3COONH4) is found to be optimal for Mo deposition 33]. However, our first attempt to deposit Mo from concentrate LiCl solutions completely failed due to the acidic pH of the solution and the overwhelming side reaction, yielding no deposit regardless of the deposition current used. On the other hand, the second attempt to deposit Re using the concentrated acetate electrolytes with CH3COONH4 and CH3COOK also failed, where a clear solution cannot be obtained due to a low solubility of KReO₄ [39]. Because LiReO₄ has a much higher solubility than KReO₄, CH₃COOLi is then used to replace CH₃COOK and clear solutions of ReO₄ with concentrated acetate are obtained. It is worth noting that in elemental Mo deposition studies, CH₃COOK works synergistically with CH₃COONH₄ to facilitate Mo deposition while CH₃COOLi works in the opposite way slightly decreasing the Mo deposition rate. However, CH3COOK cannot be used here due to its incompatibility with ReO₄.

While the highly concentrated acetate solution with CH_3COOLi and CH_3COONH_4 enables the elemental deposition of both Mo and Re, the co-deposition of Re and Mo using this same acetate electrolyte system fails again. The two metal salts of perrhenate and molybdate cannot dissolve in the solution simultaneously, resulting in cloudy solution. This is true even after further lowering the concentrations of ReO_4^- and MoO_4^{2-} . Surprisingly, the addition of as little as 0.1 M citric acid is found

to effectively co-dissolve the two metal salts, finally enabling the study of the co-deposition of $\rm ReO_4^-$ and $\rm MoO_4^{2-}$. The cyclic voltammetry of a typical alloy electrolyte comprising 0.02 M $\rm ReO_4^-$, 0.05 M $\rm MoO_4^{2-}$, 0.4 M citric acid, 0.5 M LiAc, and 8.5 M NH₄Ac, is presented in Figure S-1 in the supplementary information. The cathodic reaction starts below -1 V and, as discussed later, the majority of cathodic current is hydrogen evolution due to the reduction of proton and water.

3.2. Effects of acetate

As discussed above, citric acid is found necessary to co-dissolve the two metal salts and enable the co-deposition of Re and Mo. Therefore, the necessity of acetate is studied first. Fig. 1 shows the partial current densities of Re and Mo at different applied current densities for two identical electrolytes except for the presence and absence of acetates. The solutions used here both contain 20 mM ReO_4^- and 50 mM MoO_4^{2-} , as well as 0.4 M citric acid. First, it is evident from Fig. 1(b) that no Mo can be deposited in absence of acetate and the films deposited therein are pure Re. Second, the Re deposition rate in absence of acetate increases almost linearly with respect to the applied current density. The linear slope of this increasement represents a constant and extremely low Faraday efficiency of about 0.08 %. It is worth noting that the concentrations of Re and Mo used in this work is low at 10's of mM range. But the partial current densities and Faraday efficiency are not limited by diffusion and the observations here reflect the kinetic behavior of the deposition. For example, MoO_4^{2-} and ReO_4^{-} anions have a diffusion coefficient of 1.98×10^{-5} and 1.46×10^{-5} cm²/s, respectively, in a dilute concentration [14]. As the diffusivity of metal ions is expected not to be significantly lowered in the concentrated solution [40], a limiting current on the order of 186 mA/cm² would be expected at a rotation rate of 1000 rpm for a kinematic viscosity up to 14 cP and a MoO₄²⁻ concentration of 50 mM. A similar limiting current of 71 mA/cm² would be expected for 20 mM ReO₄. The addition of acetate at a superhigh concentration not only enables the deposition of Mo but also increases the Re deposition rate. As shown in Fig. 1(a), Mo deposition is enabled when the applied current density reaches -100 mA/cm² and the deposition rate approximately linearly increases along with the applied current. This is consistent with the studies on elemental Mo deposition, where a high concentration of acetate is found necessary [33]. It is evident from Table 1 that the solution without acetate has a much lower pH than the one with acetate. The prevention of Mo deposition in this acidic solution is also consistent with the similar observation in acidic LiCl electrolytes mentioned above. A neutral pH with a strong buffering capacity appears to be necessary for Mo deposition. The comparison between Figs. 1(a) and 1(b) also shows that the Re partial current density doubles or even triples in presence of acetates depending

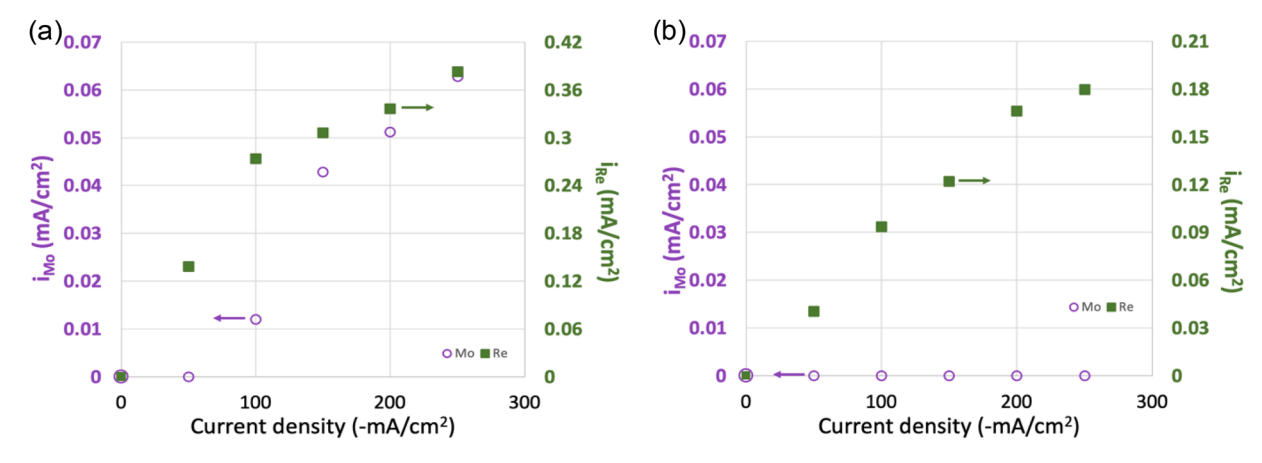


Fig. 1. Effect of current density and acetate on Re-Mo alloy electrodeposition: the partial current densities for Re and Mo as the function of applied current density (a) with 0.5 M CH_3COOLi , and 8.5 M CH_3COONH_4 ; and (b) without acetate. Both electrolytes contain 0.02 M ReO_4^- , 0.05 M MoO_4^{2-} , and 0.4 M citric acid.

on the applied current density. In addition, the deposition rate of Mo increases faster than Re, resulting in a decrease of Re content in the film from 95 at.% to 84 at.% as the deposition current density increases from 100 to 250 mA/cm 2 . Electrolytes with 0.5 M CH $_3$ COOLi and 8.5 M CH $_3$ COONH $_4$ are used for the following studies, and a high current density of -200 mA/cm 2 is used to ensure the co-deposition of both elements.

3.3. Effects of ReO₄

Re-Mo alloy deposition is further carried out to study the effects of ReO_4^- concentration. The concentrations of MoO_4^{2-} and citric acid in the solutions are fixed at 0.05 M and 0.4 M, respectively. The concentration of ReO₄ varies from 0 M to 0.05 M. The concentrations of acetates, i.e., LiAc and NH₄Ac, are fixed at 0.5 M and 8.5 M, respectively. At these concentrations, as discussed in the previous section, ReO₄ and MoO₄² ions can be completely dissolved together. Another thing worth noting is that the solubility of ReO_4^- is lower than that of MoO_4^{2-} in the electrolyte chemistry system [39], limiting the concentration range of ReO₄ in this set of studies up to 0.05 M. The solutions are maintained at room temperature (20 °C), and the natural pH's from 6.4 to 6.5 (details in Table 1) are used. The electrodeposition studies are conducted in these ReMo electrolytes at a current density of -200 mA/cm^2 for 1800s. Fig. 2(a) shows the effects of ReO₄ concentration on faradaic efficiency (FE) and Re content in films. The Re contents in alloy films, excluding the pure Mo film deposited without ReO₄, are approximately independent of the ReO₄ concentration in solution. On the other hand, the FE increases with the ReO_4^- concentration. In order to further understand the reason why the film composition remains unchanged, the partial current densities for Re and Mo are calculated and are presented in Fig. 2(b). Figure S-2 in Supplementary Information shows the same partial current densities with the error bars calculated from the five measurements across the sample diameter. The errors are relatively more pronounced for Mo than Re due to the much lower content of Mo in the film. First, the partial current density for Re increases with ReO₄ concentration. Surprisingly, the partial current density for Mo also increases with the concentration of ReO₄ concentration except for the electrolyte without any ReO₄, where Mo is deposited by itself. Furthermore, the increase of the deposition rates for Re and Mo are both approximately linear with respect to ReO₄ concentration, resulting in a nearly constant film composition as observed in Fig. 2(a). In more details, as the ReO4 concentration increases from 0.005 to 0.05 M, Re deposition rate increases from 0.14 to 0.54 mA/cm² while Mo rate increases from 0.013 to 0.066 mA/cm². This results in an approximately constant Mo/Re atomic ratio of 1/7, namely a constant Mo content at around 13 at.%, for the alloy films. This also suggests that the Mo deposition rate in the alloy electrolytes is closely related to or probably even determined by the presence of ReO₄ or the deposition of Re.

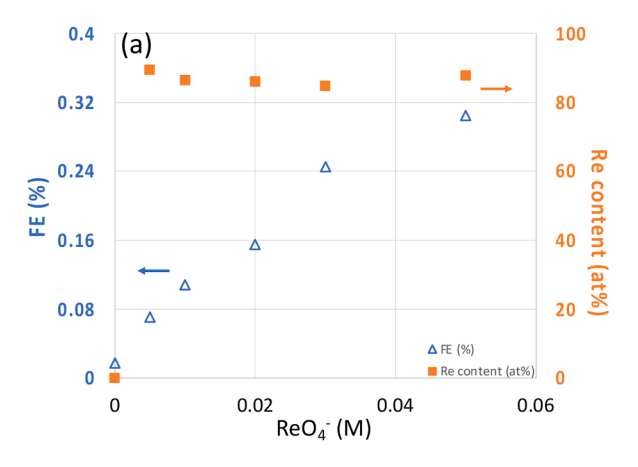
Another observation worth noting is that Mo is also deposited without ReO_4^- , resulting in pure Mo film. More importantly, the Mo deposition rate is even slightly higher than the rate when ReO_4^- is present at a low concentration (up to 0.01 M). The pH of electrolyte is not changed upon the addition of ReO_4^- , and this weak inhibition in Mo deposition rate may suggest a competitive formation or competitive surface adsorption between different complexed species involved in different deposition pathways.

3.4. Effects of MoO_4^{2-}

The effects of MoO_4^{2-} concentration on ReMo alloy deposition, i.e., the FE, film composition, and the partial current densities for Re and Mo, are shown in Fig. 3. In this set of studies, the concentrations of ReO₄ is fixed at 0.02 M. The concentrations of other constituents such as and citric acid and acetates remain the same as the previous study on ReO₄ concentration. The concentration of MoO₄² varies from 0 M to 0.07 M. The deposition is also carried at a current density of -200 mA/cm^2 for 1800s. Re content in film decreases from 100 at.% to 80 at.% as MoO_4^2 concentration increases up to 0.07 M. The FE remains low and largely unchanged with a small variation. The partial current density in Fig. 3 (b) shows that the FE closely follows the deposition rate of Re. While the partial current density for Mo increases with MoO₄²⁻ concentration, it remains much lower than the Re deposition rate, which remains approximately unchanged with a same small fluctuation as the FE. A close look at Fig. 1(b) reveals that no Mo is deposited even when the MoO₄²⁻ concentration increases to 0.01 M. This appears to be consistent with the observation discussed above in Fig. 2, where the presence of ReO₄ inhibits Mo deposition compared with Mo elemental deposition. This is believed to result from the depletion of a Re-free intermediate species for Mo deposition or the adsorption of a Re-containing intermediate species blocking the electrode surface and inhibiting Mo deposition. Another detailed feature is that the FE and Re deposition partial current reach a maximum at a MoO_4^{2-} concentration between 0.2 and 0.3 M. While more detailed studies will be required in future, this maximum may reflect the presence and different behaviors of various complexed species in the electrolyte.

3.5. Effects of citric acid

As discussed previously in the electrolyte section, the presence of citric acid is necessary to co-dissolve Re and Mo salts to obtain a clear alloy solutions. In this set of studies, the co-deposition is carried out using solutions containing $0.02~M~ReO_4^-$, $0.05~M~MoO_4^{2-}$, 0.5~M~LiAc, $8.5~M~NH_4Ac$, and various citric acid concentrations. The natural pHs of solution are used, which decrease from 7.1 to 6.1 as the citric acid



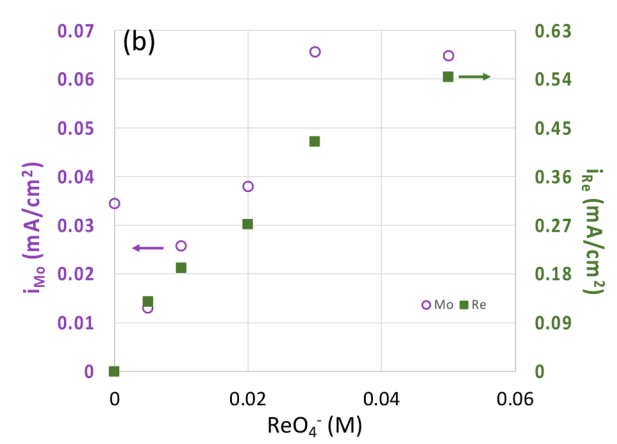


Fig. 2. Effects of ReO_4^- concentration on Re-Mo alloy electrodeposition: (a) the faradaic efficiency and Re content in ReMo deposits, and (b) partial current densities of Re and Mo, as a function of ReO_4^- concentration. The solutions contain 0.05 M MoO_4^{2-} , 0.4 M citric acid, 0.5 M LiAc, and 8.5 M NH_4Ac .

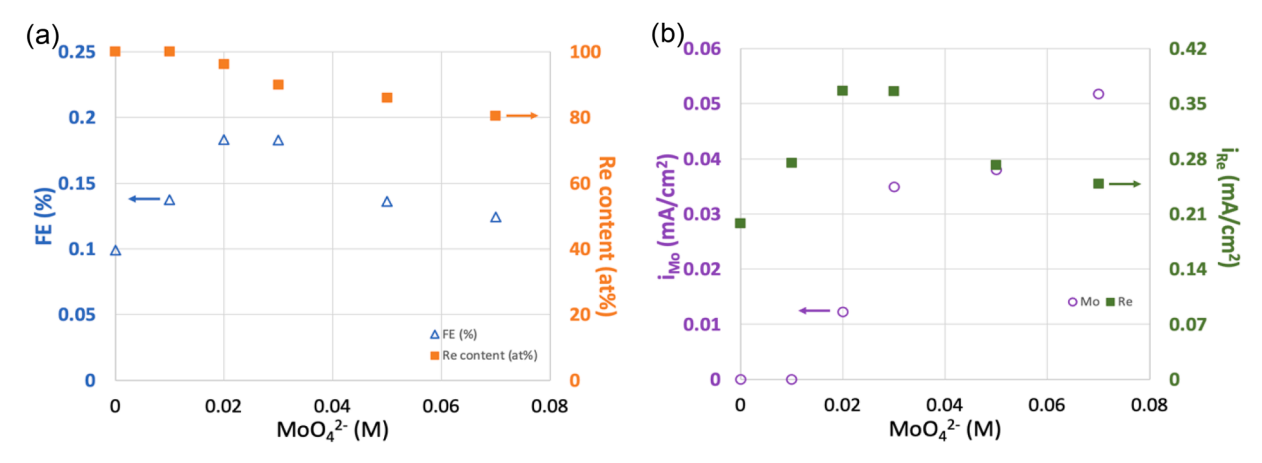


Fig. 3. Effects of MOO_4^{2-} concentration on Re-Mo alloy electrodeposition: (a) the faradaic efficiency and Re content in Re-Mo deposits, and (b) partial current densities for Re and Mo, as a function of MOO_4^{2-} concentration. The solutions contain 0.02 M ReO_4^{-} , 0.4 M citric acid, 0.5 M LiAc, and 8.5 M NH_4Ac .

concentration increases from 0.1 to 0.9 M. A same constant current density of -200 mA/cm^2 is used in the study. As Fig. 4(a) shows, the FE of deposition is still below 1 %. Yet, it appears to have a maximum efficiency with the citric acid concentration between 0.2 to 0.4 M. The Re content in film increases with the concentration of citric acid. However, a detailed inspection show approximately a step change from about 80 at.% Re to 100 at.% as citric acid concentration increases from 0.4 to 0.7 M. While the Re content does increase before this step jump, the increase is very minimum, from 77 % to 84 %. Fig. 4(b) shows the dependence of partial current densities for Re and Mo on the citric acid concentration. The data points at 0 M citric acid are manually added to indicate that a clear alloy solution cannot be obtained. There are clearly two regions within the citric acid concentration range studied. The first region spans between 0.1 to 0.4 M, where both Mo and Re can be deposited. In this region, the deposition of Mo and Re both showed a maximum rate at about 0.2 M citric acid. Furthermore, the ratio between the deposition rates of Re and Mo remains relatively stable between 4 and 7, resulting in an approximately constant film composition with 77 at.% to 84 at.% Re. The second region corresponds to a citric acid concentration of 0.7 M or above, where Mo cannot be deposited, resulting in pure Re films.

3.6. Discussion on alloy deposition

The electrodeposition of Mo and Re from aqueous solutions are challenging, both accompanied by high surface activity toward hydrogen evolution reactions resulting in low faradaic efficiencies. Furthermore, the deposition potentials of the two metals are far apart.

While the deposition of elemental Mo occurs at potentials more negative than -1.3 V after ohmic correction [33], the deposition rate of elemental Re decreases at potentials more negative than -1.1 V due to the further reduction of Re metal to rhenide anions [34,41]. This renders the co-deposition more difficult. However, the electrodeposition of both Mo and Re is facilitated by iron group metals, such as Fe and Co. Among them, the enhancement of Mo deposition rate is often observed in presence of a multidentate complexing ligand such as citric acid and the mechanism is attributed to the formation and reduction of coordinated complexes with both molybdate anion and iron-group cations. On the other hand, the enhancement of Re deposition by iron-group metals can be observed both in presence and in absence of ligands, possibly involving different mechanisms. A displacement reaction between Re (VII) and electro-reduced iron-group metal atoms on surface was proposed in citrate solutions, providing an additional pathway and an enhanced rate of Re deposition [28,42]. On the other hand, the presence of citrate anion alone was also found to adsorb on the electrode surface, inhibit charge transfer, and suppress metal deposition. A different mechanism of the enhanced Re deposition rate in presence of iron group metal was therefore proposed to result from the change of the adsorbate speciation from proton coordinated citrate to iron-group metal cation coordinated citrate [43]. This change eases the reduction of metal-ligand complex adsorbate, unblocking the electrode surface and facilitating Re deposition. In addition, the enhancement in Re deposition is also observed in simple electrolytes with only sulfate and chloride. The further reduction of Re into rhenide anion (Re⁻) at highly negative potential was found to be impeded due to the stabilization of Re by

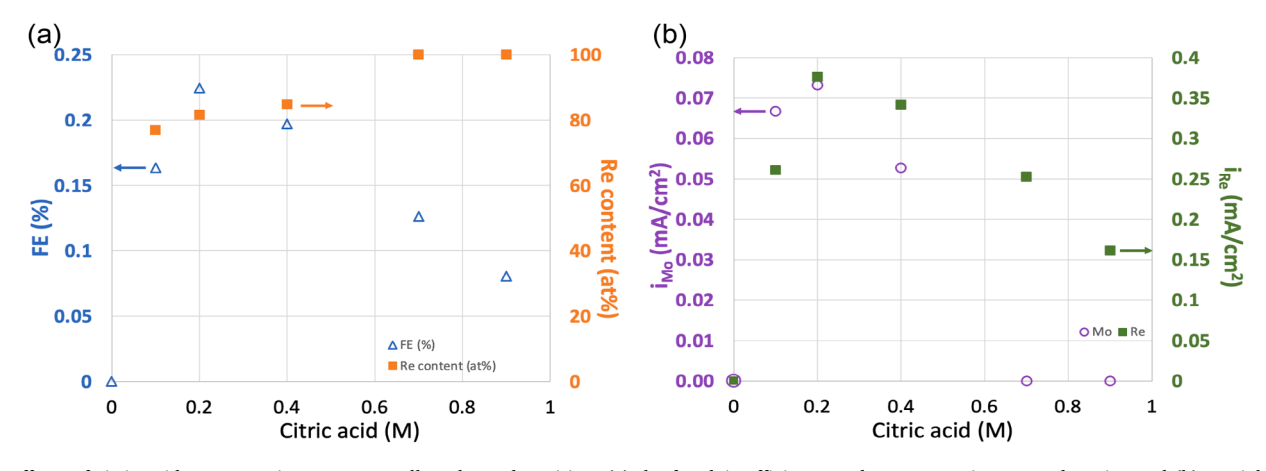


Fig. 4. Effects of citric acid concentration on Re-Mo alloy electrodeposition: (a) the faradaic efficiency and Re content in Re-Mo deposits, and (b) partial current densities for Re and Mo, as a function of citric acid concentration. The solutions contain 0.02 M ReO_4^2 , $0.05 \text{ M MoO}_4^{2-}$, 0.5 M LiAc, and 8.5 M NH_4 Ac.

alloying with iron-group metal [25].

No iron-group metals or any simple metal cations are used in this study. Instead, molybdate and perrhenate are both oxometallate anions with a similar structure. Furthermore, the electronegativity of Mo and Re are close to each other [44] and a displacement reaction is unlikely to occur. As the perrhenate concentration increases, the deposition rates of Re and Mo both increases at an approximately similar ratio (Section 3.3). On the other hand, the increase of molybdate only results in an increase of Mo deposition rate. The Re deposition rate stays approximately same or with minimum fluctuation (Section 3.4). These observations suggest that the deposition of Mo in this study requires or highly depends on the deposition of Re, while the deposition of Re can proceed alone and is independent of the deposition of Mo. Furthermore, the deposition rates of Re and Mo are highly correlated as far as the citric acid concentration is concerned, where a maximum rate is observed for both metals at an intermediate citrate concentration of about 0.2 M (Section 3.5). The above observations suggest that one or more hybrid complex intermediate species with both molybdate and perrhenate is involved in the deposition pathway.

Molybdate is known to form a large variety of complex structures with the citrate ligand and the stability constants have been systematically studied before [45,46]. Each multidentate citrate ligand can coordinate with multiple molybdate anions and each molybdate coordinates with multiple citrate ligands as well, resulting in cross-linked complex structures [47]. While the specific details may vary and the stability constants are unavailable, the perrhenate anion has been proposed to coordinate with citrate ligands in a similar fashion as molybdate [48]. Fig. 5(a) shows the Mo speciation in an electrolyte with 0.05 M Molybdate and 0.4 M citrate at different pH, computed using the stability constants from literature [49]. Here the complexing effect of monodentate acetate is assumed to be negligible and is folded under the species free-MoO₄²⁻. A speciation notation (k,m,n) is used to represent (MoO₄²⁻)_k(HCit³⁻)_mH_n, where the three carboxyl oxygen and one hydroxyl oxygen of a citrate molecule are all considered as potential electron donors for chelating. To simplify the comparison, the species are further categorized using the Mo:Cit ratio, i.e. the k:m ratio, with the proton coordination ignored, and are summarized in Fig. 5(b). While the computations are based on molybdate without perrhenate, the behavior of MoO_4^{2-} and ReO_4^{-} are proposed to be similar [48] and both oxometallates are believed to preferably complex with citrate with a 1:1 stoichiometry, namely as $(MoO_4^{2-})(HCit^{3-})$, $(MoO_4^{2-})_2(HCit^{3-})_2$, or even $(MoO_4^{2-})_4(HCit^{3-})_4$, regardless of the electrolyte pH between 6 and 7.

Based on the above observation and discussion, a hybrid complex, such as $(MoO_4^{2-})(ReO_4^{-})$ $(HCit^{3-})_2$, is believed to form. Other hybrid complexes similar to $(MoO_4^{2-})_4(HCit^{3-})_4$, namely, $(MoO_4^{2-})_x(ReO_4^{-})_4$, $(HCit^{3-})_4$, can also form depending on the stability constants. These hybrid complexes apparently play a critical role in Mo deposition either as an intermediate in solution, an adsorbate on electrode surface, or

even in a partially reduced form on electrode surface. While free MoO_4^{2-} and certain Re-free molybdate-citrate complexes may still be present in the solution, they are believed not to significantly contribute to the Mo deposition rate during the alloy co-deposition. The amount of the hybrid complexes strongly depends on the concentrations of both ReO4 and MoO_4^{2-} , and so does the Mo deposition rate. On the other hand, while the reduction of such hybrid complexes also results in Re deposition, free ReO4 and Mo-free complexes between Re and citrate such as (ReO₄)_k(HCit³)_m are still present in the electrolyte, enabling additional pathways for Re deposition. Furthermore, the Re deposition rate through these routes is believed to be much higher than the rate through hybrid complexes. This results from a much smaller fraction for hybrid complexes as compared with the Mo-free species or a much sluggish reduction kinetics for the former species than the latter. As a result, the overall Re deposition rate is largely independent of MoO₄²⁻ concentration but strongly correlates with ReO₄ concentration. Another detailed feature in Fig. 3 is that the Re deposition rate and Faraday efficiency reach a maximum at a MoO_4^{2-} concentration between 0.2 and 0.3 M (Section 3.4). As the hybrid complex structures start to form upon the addition of MoO_4^{2-} into Re-citrate electrolyte, a speciation shift is expected to occur as the MoO_4^{2-} concentration increases. In other words, the x values in $(MoO_4^{2-})_x(ReO_4^{-})_{2-x}(HCit^{3-})_2$ and $(MoO_4^{2-})_x(ReO_4^{-})_4$. $_{\rm x}$ (HCit³⁻)₄ increase. The maximum observed at 0.2 to 0.3 M MoO₄²⁻ is believed to result from the different speciation and different reduction rates of those different species. On the other hand, as citrate concentration varies (Section 3.5), similar change in the speciation is also expected and similar maximum is observed as well in Fig. 4. A systematic chemical analysis will be needed to understand the quantitative details of the tertiary Molybdate-Perrhenate-Citrate electrolyte system. Nevertheless, the observations in the above studies suggest that certain hybrid complex speciation promotes or inhibits the deposition, and such complexes reach a maximal or minimal concentration depending on the stability constants and the concentrations of different constituents.

3.7. Electrodeposited ReMo alloy films

The alloy films deposited are of a Re content between 80 and 90 at.% across all the concentrations and conditions used in the above studies. Fig. 6(a) shows the typical morphology of such a film with a Mo content of 18 at.% and a thickness of 240 nm deposited on Cu disc electrode from an electrolyte comprising 0.4 M citric acid, 20 mM ${\rm ReO_4^-}$ and 50 mM ${\rm MoO_4^{2-}}$. A continuous film with nodular grains up to 200 nm in diameter is observed. The small grooves appear to replicate the polishing grooves of the Cu disc. Fig. 6(b) shows the resistance of a duplicated film with 16 at.% Mo deposited on a silicon coupon with Au pattern. As the temperature sweeps from 10 K to 2 K, a superconducting transition at a critical temperature (${\rm T_c}$) of 5.7 K is observed, same as the pure Re films reported previously [23]. The grain structure of this as-deposit film is

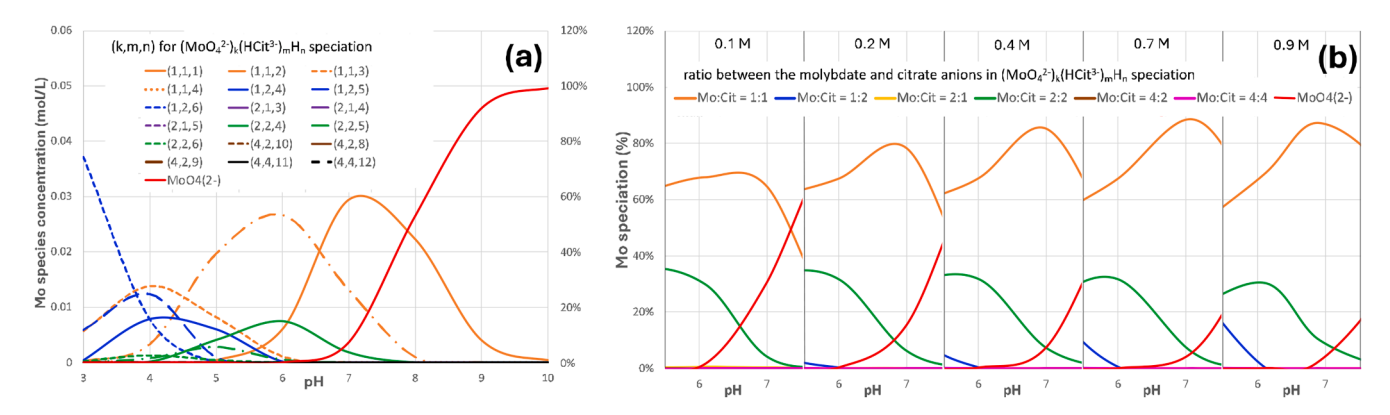


Fig. 5. The speciation of 0.05 M MoO₄²⁻ in citric acid electrolytes at different pH calculated from stability constants. The electrolytes comprise (a) 0.4 M citric acid at different pH from 3 to 10, and (b) various concentrations of citric acid at pH between 5.5 to 7.5.

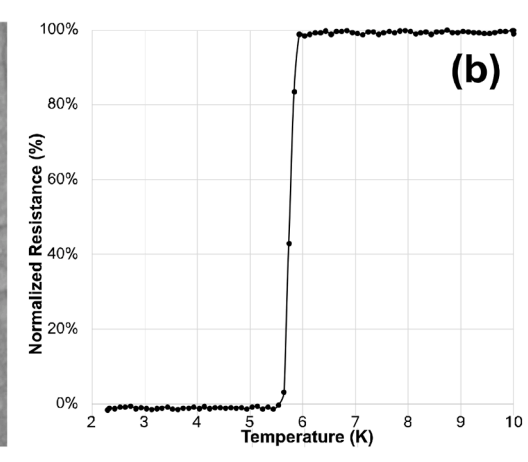


Fig. 6. (a) Top-down SEM micrograph and (b) film resistance at cryogenic temperatures of a typical ReMo film deposited from electrolytes comprising 0.02 M ReO₄⁻, 0.05 M MoO₄², 0.4 M citric acid, 0.5 LiAc, and 8.5 M NH₄Ac.

also similar to pure Re, remaining amorphous or nanocrystalline and resulting in this enhanced transition temperature as compared with crystalline Re. The presence of up to 16 at.% Mo in Re apparently does not have significant impact on the superconductivity, different from the doping with Co and Fe [25,26].

While potassium doped oxides of Re and Mo was also reported to be superconducting [50], the $T_{\rm c}$ observed in those oxides are much lower than the MoRe alloy here. In addition, ReMo films are deposited in this study using electrolytes with no potassium salts added. On the other hand, the same oxides doped with sodium were found to show no superconductivity [50]. More systematic studies on the characterization of electrodeposited MoRe alloys will be carried out and published separately. This amorphous film recrystallizes to an hexagonal close packed structure intrinsic to elemental Re upon high temperature annealing. While the lack of oxide crystal cannot completely rule out the presence of oxygen, the film is believed to be predominantly metallic and the $T_{\rm c}$ observed here corresponds to the behavior of metallic alloy of MoRe.

4. Conclusions

The electrochemical co-deposition of ReMo alloy is reported as an alternative route to fabricate the superconducting alloy films. The effects of applied current density and the concentrations of perrhenate, molybdate, acetate, and citrate on the alloy co-deposition are systematically studied. While a high concentration of acetates is required for Mo deposition benefitting from a strong pH buffering capacitance of acetates, the presence of citric acid is necessary to co-dissolve ReO₄ and MoO_4^{2-} enabling the co-deposition. Furthermore, the Mo deposition rate in alloy closely follows the Re deposition when ReO₄ concentration changes. Contrarily, varying MoO_4^{2-} concentration only changes the Mo deposition rate but not Re rate. A hybrid citrate complex with both Re and Mo oxometallates is proposed to enable the Mo reduction, where the reduction of Mo and Re occurs together. On the other hand, Re deposition occurs through multiple pathways involving hybrid complex or other Mo-free species such as ReO₄ or ReO₄-citrate complex. While the Faraday efficiency is low for ReMo alloy deposition, continuous film with amorphous grain structure can be obtained with various Mo content doped in Re. The superconducting transition for films up to 16 at.% Mo is found similar to pure Re, presenting an amorphous grain structure and an enhanced T_c around 5.7 K. The presence of Mo doping does not compromise the superconductivity of electrodeposited Re in contrast to iron-group metal dopants, potentially providing a method to tune the thermal stability of the enhanced T_c.

CRediT authorship contribution statement

Quanhong Liu: Writing – original draft, Methodology, Investigation, Formal analysis, Data curation. **Qiang Huang:** Writing – review & editing, Writing – original draft, Supervision, Project administration, Investigation, Funding acquisition, Formal analysis, Conceptualization.

Declaration of competing interest

The authors declare that they have no known competing financial interests or personal relationships that could have appeared to influence the work reported in this paper.

Data availability

Data will be made available on request.

Acknowledgement

This work is supported by the National Science Foundation through grants 1941820. The Core Analytical Facility of Alabama Material Institute at the University of Alabama is acknowledged for the access and training of equipment for materials characterization. The glass shop at the University of Alabama is acknowledged for making the electrochemical cells.

Supplementary materials

Supplementary material associated with this article can be found, in the online version, at doi:10.1016/j.electacta.2024.144761.

References

- A.A. Woolf, An outline of rhenium chemistry, Q. Rev. Chem. Soc. 15 (1961) 372, https://doi.org/10.1039/gr9611500372.
- [2] J.W. Fergus, Wesley P. Hoffmann, High Temperature Materials and Mechanisms, CRC Press, 2014, pp. 39–67.
- [3] S.M. Augustine, W.M.H Sachtler, On the mechanism for the platinum-catalyzed reduction of rhenium in PtRe γ-Al2O3, J. Catal. 116 (1989) 184–194, https://doi. org/10.1016/0021-9517(89)90085-7.
- [4] P. Clark, B. Dhandapani, S.T. Oyama, Preparation and hydrodenitrogenation performance of rhenium nitride, Appl. Catal. A Gener. 184 (1999) L175–L180, https://doi.org/10.1016/s0926-860x(99)00095-2.
- [5] G. Jin, B.s. Xu, H.d. Wang, Q.f. Li, S.c. Wei, Tribological properties of molybdenum coatings sprayed by electro-thermal explosion directional spraying, Surf.Coat. Technol. 201 (2007) 6678–6680, https://doi.org/10.1016/j.surfcoat.2006.09.028.
- [6] D. Gall, Electron mean free path in elemental metals, J. Appl. Phys. 119 (2016) 085101, https://doi.org/10.1063/1.4942216.

- [7] V. Founta, et al., Properties of ultrathin molybdenum films for interconnect applications, Materialia (Oxf) 24 (2022) 101511, https://doi.org/10.1016/j. mtla 2022 101511
- [8] D.S. Gardner, J. Onuki, K. Kudoo, Y. Misawa, Q.T. Vu, Encapsulated copper interconnection devices using sidewall barriers, Thin. Solid. Films. 262 (1995) 104–119, https://doi.org/10.1016/0040-6090(95)05838-9.
- [9] M. Laribi, A.B. Vannes, D. Treheux, Study of mechanical behavior of molybdenum coating using sliding wear and impact tests, Wear. 262 (2007) 1330–1336, https:// doi.org/10.1016/j.wear.2007.01.018.
- [10] A. Fernández Guillermet, Critical evaluation of the thermodynamic properties of molybdenum, Int. J. Thermophys. 6 (1985) 367–393, https://doi.org/10.1007/ BF00500269
- [11] J.K. Hulm, Superconductivity of pure metallic rhenium, Phys. Rev. 94 (1954) 1390–1391, https://doi.org/10.1103/physrev.94.1390.2.
- [12] D.P. Pappas, et al., Enhanced superconducting transition temperature in electroplated rhenium, Appl. Phys. Lett. 112 (2018), https://doi.org/10.1063/ 1.5027104
- [13] J.K. Hulm, B.B. Goodman, Superconducting properties of rhenium, ruthenium, and osmium, Phys. Rev. 106 (1957) 659–671, https://doi.org/10.1103/ PhysRev 106 659
- [14] D.R. Lide, CRC Handbook of Chemistry and Physics, 85th edn, CRC Press, 2004.
- [15] G. Bergmann, Amorphous metals and their superconductivity, Phys. Rep. 27 (1976) 159–185, https://doi.org/10.1016/0370-1573(76)90040-5.
- [16] M.M. Collver, R.H. Hammond, Superconductivity in "Amorphous" transition-metal alloy films, Phys. Rev. Lett. 30 (1973) 92–95, https://doi.org/10.1103/ physrevlett.30.92.
- [17] H. Okamoto, T. Massalski, Binary Alloy Phase Diagrams, 12, ASM International, Materials Park, OH, USA, 1990, pp. 3528–3531.
- [18] E. Bucher, F. Heiniger, J. Muheim, J. Muller, Superconductivity and electronic properties of transition metal alloys, Rev. Mod. Phys. 36 (1964) 146–149, https://doi.org/10.1103/RevModPhys.36.146.
- [19] E. Lerner, J.G. Daunt, Thermal and electrical conductivities of Mo-Re alloys in the superconducting and normal states, Phys. Rev. 142 (1966) 251–258, https://doi. org/10.1103/physrev.142.251.
- [20] L.R. Testardi, J.J. Hauser, M.H. Read, Enhanced superconducting Tc and structural transformation in Mo-Re alloys, Solid. State Commun. 9 (1971) 1829–1831, https://doi.org/10.1016/0038-1098(71)90100-1.
- [21] C.W. Chu, W.L. McMillan, H.L. Luo, Superconductivity of Re-Os, Re-Ru, Ru-Os, and Re-W hcp alloy systems and slightly doped Re, Phys. Rev. B 3 (1971) 3757–3762, https://doi.org/10.1103/physrevb.3.3757.
- [22] T. Shang, et al., Structure and superconductivity in the binary Re_{1-x}Mo_x alloys, Phys. Rev. Mater. 3 (2019) 024801, https://doi.org/10.1103/ PhysRevMaterials.3.024801.
- [23] Q. Huang, Y. Hu, Electrodeposition of superconducting Rhenium with Water-in-Salt Electrolyte, J. Electrochem. Soc. 165 (2018) D796–D801, https://doi.org/10.1149/2.0261816jes.
- [24] W.D. Sides, et al., Grain growth and superconductivity of rhenium electrodeposited from water-in-salt electrolytes, J. Appl. Phys. 127 (2020) 085301, https://doi.org/ 10.1063/1.5139909
- [25] S. De, W.D. Sides, T. Brusuelas, Q. Huang, Electrodeposition of superconducting rhenium-cobalt alloys from water-in-salt electrolytes, J. Electroanalyt. Chem. 860 (2020) 113889, https://doi.org/10.1016/j.jelechem.2020.113889.
- [26] B. Malekpouri, K. Ahammed, Q. Huang, Electrodeposition and superconductivity of rhenium-iron alloy films from water-in-salt electrolytes, J. Alloys. Compd. 912 (2022) 165077, https://doi.org/10.1016/j.jallcom.2022.165077.
- [27] A. Naor, N. Eliaz, L. Burstein, E. Gileadi, Direct experimental support for the catalytic effect of iron-group metals on electrodeposition of rhenium, Electrochem. Solid State Lett. 13 (2010) D91–D93, https://doi.org/10.1149/1.3489532.
- [28] A. Naor, N. Eliaz, E. Gileadi, Electrodeposition of rhenium-nickel alloys from aqueous solutions, Electrochim. Acta 54 (2009) 6028–6035, https://doi.org/ 10.1016/j.electacta.2009.03.003.
- [29] E.J. Podlaha, D.Induced Landolt, Codeposition: I. An experimental investigation of Ni-Mo Alloys, J. Electrochem. Soc. 143 (1996) 885–892, https://doi.org/10.1149/ 1.1836553.

- [30] E.J. Podlaha, D. Landolt, Induced codeposition: III. Molybdenum alloys with nickel, cobalt, and iron, J. Electrochem. Soc. 144 (1997) 1672–1680, https://doi. org/10.1149/1.1837658.
- [31] N. Eliaz, E. Gileadi, Modern Aspects of Electrochemistry, 42, Springer, New York, 2008, pp. 191–301.
- [32] Y.S. Yapontseva, V.S. Kublanovsky, O.A. Vyshnevskyi, Electrodeposition of CoMoRe alloys from a citrate electrolyte, J. Alloys. Compd. 766 (2018) 894–901, https://doi.org/10.1016/j.jallcom.2018.07.018.
- [33] Q. Liu, Q. Huang, Electrodeposition of molybdenum from water-in-acetate electrolytes, J. Electrochem. Soc. 171 (2024) 062510, https://doi.org/10.1149/ 1945-7111/ad59c8.
- [34] Q. Huang, T.W. Lyons, Electrodeposition of rhenium with suppressed hydrogen evolution from water-in-salt electrolyte, Electrochem. Commun. 93 (2018) 53–56, https://doi.org/10.1016/j.elecom.2018.06.003.
- [35] A. Haftbaradaran, N. Parvini-Ahmadi, S. Yazdani, Electrodeposition and characterization of metallic molybdenum from aqueous electrolytes containing high acetate concentrations, Surf. Coat. Technol. 324 (2017) 1–6, https://doi.org/ 10.1016/j.surfcoat.2017.05.024.
- [36] S.N. Hasan, M. Xu, E. Asselin, Electrosynthesis of metallic molybdenum from water deficient solution containing molybdate ions and high concentrations of acetate, Surf. Coat. Technol. 357 (2019) 567–574.
- [37] T.J. Morley, et al., The deposition of smooth metallic molybdenum from aqueous electrolytes containing molybdate ions, Electrochem. Commun. 15 (2012) 78–80, https://doi.org/10.1016/j.elecom.2011.11.026.
- [38] R. Syed, et al., Electrodeposition of thick metallic amorphous molybdenum coating from aqueous electrolyte, Surf. Coat. Technol. 261 (2015) 15–20, https://doi.org/ 10.1016/j.surfcoat.2014.11.073.
- [39] W.T. Smith Jr., S.H Long, The salts of perrhenic acid. i. the alkali metals and ammonium1, J. Am. Chem. Soc. 70 (1948) 354–356, https://doi.org/10.1021/ ja01181a110.
- [40] S. De, et al., Electrochemical behavior of protons and cupric ions in water in salt electrolytes with alkaline metal chloride, Electrochim. Acta 338 (2020) 135852, https://doi.org/10.1016/j.electacta.2020.135852.
- [41] M. Pourbaix, Atlas of Electrochemical Equilibria in Aqueous Solutions 2d English edn, National Association of Corrosion Engineers, 1974.
- [42] A. Naor, N. Eliaz, E. Gileadi, Electrodeposition of alloys of rhenium with iron-group metals from aqueous solutions, J. Electrochem. Soc. 157 (2010) D422, https://doi. org/10.1149/1.3430084.
- [43] F. Contu, S.R. Taylor, Further insight into the mechanism of Re-Ni electrodeposition from concentrated aqueous citrate baths, Electrochim. Acta 70 (2012) 34–41. https://doi.org/10.1016/j.electacta.2012.03.010.
- [44] W. Gordy, W.O. Thomas, Electronegativities of the elements, J. Chem. Phys. 24 (1956) 439–444
- [45] J.J. Cruywagen, R.F. Van de Water, Complexation between molybdenum(VI) and citrate: a potentiometric and calorimetric investigation, Polyhedron.Polyhedron. 5 (1986) 521–526, https://doi.org/10.1016/S0277-5387(00)84958-X.
- [46] Y.Z. Hamada, N. Bayakly, D. George, T. Greer, Speciation of molybdenum(VI)-citric acid complexes in aqueous solutions, Synthes. React. Inorgan. Metal Organ. Nano Metal Chem. 38 (2008) 664–668, https://doi.org/10.1080/15533170802371323
- [47] N.W. Alcock, et al., Complexation between molybdenum(VI) and citrate: structural characterisation of a tetrameric complex, K4[(MoO2)4O3(cit)2]·6H2O, J. Chem. Soc. Dalton Transact. (1990) 707–711, https://doi.org/10.1039/DT9900000707.
- [48] J. Vajo, et al., Facile electroreduction of perrhenate in weakly acidic citrate and oxalate media, Inorg. Chem. 20 (1981) 3328–3333.
- [49] J.J. Cruywagen, E.A. Rohwer, G.F.S. Wessels, Molybdenum(VI) complex formation—8. Equilibria and thermodynamic quantities for the reactions with citrate, Polyhedron.Polyhedron. 14 (1995) 3481–3493, https://doi.org/10.1016/ 0277-5387(95)00210-J.
- [50] A.W. Sleight, T.A. Bither, P.E. Bierstedt, Superconducting oxides of rhenium and molybdenum with tungsten bronze type structures, Solid. State Commun. 7 (1969) 299–300, https://doi.org/10.1016/0038-1098(69)90404-9.